Wigner Monte Carlo simulation of phonon-induced electron decoherence in semiconductor nanodevices

Damien Querlioz,* Jérôme Saint-Martin, Arnaud Bournel, and Philippe Dollfus
Institut d'Electronique Fondamentale, CNRS, University Paris-Sud, 91405 Orsay, France
(Received 26 July 2008; revised manuscript received 29 August 2008; published 6 October 2008)

This paper examines the phonon-induced electron decoherence in semiconductor nanostructures and nanodevices within the Wigner transport equation, solved using a particle Monte Carlo technique. The Wigner-Boltzmann formalism is first established as a relevant and original approach to modeling electron quantum decoherence in semiconductors. The simulation of the time evolution of a free wave-packet then allows analyzing the competition between decoherence and wave-packet expansion in a semiconductor. It is additionally argued that decoherence occurs faster than in the widely studied case of quantum Brownian motion. The simulation of a wave packet interacting with a tunnel barrier allows studying the electron localization induced by decoherence. The case of a wave packet interacting with a double barrier puts forward the mechanism of decoherence-induced transition from resonant to sequential transport through a bound state. Finally the simulation of resonant tunneling devices shows how these phenomena take place in nanodevices and highlights the transition from the quantum transport regime to the semiclassical transport regime induced by phonon scattering.

DOI: 10.1103/PhysRevB.78.165306 PACS number(s): 73.63.−b, 85.35.−p, 03.65.Yz, 02.70.Uu

I. INTRODUCTION

The physics of transport in solid-state electron devices has been deeply and successfully investigated in the frame of the semiclassical approximations which consider electrons as localized particles experiencing recurrent scattering events by interaction with phonons or impurities. However, in modern nanodevices, the active region becomes typically smaller than the electron wavelength and mean-free path even at room temperature. The wavelike nature of electrons is thus to be considered within quantum transport models. All sources of decoherence effects deserve careful analysis to establish the connection between the ideal quantum system and the semiclassical world which are not of course strictly separated. Beyond the analysis of nanodevice operation, the study of decoherence is crucial to assess the possible realization of quantum information processing solid-state devices.

Different works have been performed on decoherence in solid-state nanodevices. Decoherence in the transport through quantum dots has been widely discussed, in particular within the concept of pointer states.[1] Knezevic[2] recently investigated the decoherence induced by contact coupling in ballistic structures. The time evolution of the entanglement between two electrons was analyzed by solving the time-dependent Schrödinger equation (Ref. 3 and references therein). Our work focuses here on the phonon-induced decoherence which is expected to be very important in electron devices operating at room temperature. Decoherence is here understood as the decay of spatial coherences of the wave packet, captured by the off-diagonal elements of the density matrix in the spatial coordinate representation. In recent works, the electron decoherence induced by electron-phonon interaction has for example been considered in a molecular conductor in the language of Landauer's approach of transport by means of Green's function calculation.[4] This decoherence effect on an electron has been investigated in a bulk semiconductor by evaluating the time evolution of the generalized Wigner's function of the electron-phonon system[5] for a single electron or phonon-scattering event.

This paper investigates decoherence induced by the coupling to the full phonon bath in an electron device operating at room temperature. We discuss the competition between coherence and decoherence for different typical transport situations in semiconductor structures and devices where electrons interact with phonons. The Wigner transport formalism is used to take advantage of its strong analogy with the semiclassical Boltzmann's approach and to show how the phonon-induced decoherence and localization[6] of electrons can explain the emergence of semiclassical transport in a nanodevice. Another major advantage is that the Wigner's formalism offers a straightforward access to the nondiagonal terms of the density matrix which provides a visualization of decoherence phenomena.

The paper is organized as follows. We first introduce the Wigner-Boltzmann equation as an original approach to model decoherence and the Monte Carlo technique used to solve it. The case of a free wave-packet then allows us to study the competition between decoherence and wave-packet expansion in semiconductors to compare this decoherence situation with the widely studied quantum Brownian motion case. We then analyze the cases of the interaction of a wave-packet with a single and a double tunnel barrier. Finally the simulation of resonant tunneling devices shows how these phenomena take place in realistic nanodevices and the transition between the quantum transport regime and the semiclassical transport regime. The coupling of Boltzmann and Wigner Monte Carlo simulations allows us to examine the quantum to semiclassical transition resulting from phonon scattering.

II. DERIVATION OF THE WIGNER-BOLTZMANN EQUATION FROM THE DECOHERENCE POINT OF VIEW

A. Wigner-Boltzmann equation

In recent works, quantum transport in electron devices in the presence of phonon scattering has been essentially studied by using different formalisms: the density matrix, the nonequilibrium Green's functions (NEGFs), and the Wigner function (WF).

The density matrix in the reciprocal space representation allows a very precise treatment of the electron-phonon coupling Hamiltonian, including collisional broadening and retardation and intracollisional field effect,[7–9] but does not allow the study of space-dependent phenomena. Nanodevice simulation is however possible with the density matrix using Pauli master's equation.[10,11] The density matrix is then expressed in a set of wave functions providing a basis of the system, and electron-phonon coupling is modeled at the Fermi golden rule level. The modeling of the contacts[10,12] and of the transient regime[10,13] raises difficult issues in this model and it is believed to be limited to devices smaller than the electron dephasing length.[11]

In the NEGF formalism, the most simple approach to including phonon scattering is the phenomenological Büttiker probe technique,[14] which is widely used for nanodevice simulation.[15–17] The Büttiker probe formalism may be derived from actual scattering Hamiltonians,[4,18] but it cannot model the detailed momentum and energy exchanges when several phonon modes are involved in scattering processes. More advanced formulations of electron or phonon scattering are possible within the Green's function formalism using perturbation theory[19] and are progressively introduced into nanodevice simulation.[20,21]

Another possibility to model quantum transport with scattering is the Wigner formalism.[22] The Wigner function is defined as a differential Fourier transform of the density matrix of the electrons.[23] It has been commonly used for decoherence studies in atomic physics,[24,25] as well as for device modeling.[26–34] In the frame of semiconductor device analysis it offers two major advantages over the density matrix and NEGF. First, in a semiclassical situation the WF, defined in the phase space, is equivalent to the distribution function described by the Boltzmann formalism (which is nothing but the classical limit of the Wigner quantum theory).[29] Second, it is naturally a time-dependent formulation, which makes it very convenient to study the dynamics of decoherence, all the more because it gives easy access to the electron-density matrix in the spatial coordinate representation by inverse Fourier transform of the WF.

This paper intends to describe how interaction of the electrons with the phonon bath leads to decoherence in nanodevices. We first establish the Wigner-Boltzmann equation as a relevant technique to study decoherence. We consider an electron coupled to a phonon mode $\mathbf{q}$ of energy $E_0=\hbar\omega_0$ and occupation number n. Using the conventional phase-space coordinates $(\mathbf{r},\mathbf{k})$, the generalized Wigner function of the system including the electron and the phonon mode obeys the Wigner transport equation which reads, as demonstrated in Ref. 23,

$$\left[\frac{\partial}{\partial t}+\frac{\hbar\mathbf{k}}{m}\frac{\partial}{\partial\mathbf{r}}-Q+i\omega_0(n-n')\right]f_w(\mathbf{r},\mathbf{k},n,n',t)=Cf_w(\mathbf{r},\mathbf{k},n,n',t), \tag{1}$$

where the effect of the potential V is included in the quantum evolution term

$$Qf_w(\mathbf{r},\mathbf{k},n,n',t)=\frac{1}{i\hbar(2\pi)^3}\int d\mathbf{k}'f_w(\mathbf{r},\mathbf{k}+\mathbf{k}',n,n',t)\int d\mathbf{r}'e^{-i\mathbf{k}'\mathbf{r}'}\left[V\left(\mathbf{r}+\frac{\mathbf{r}'}{2}\right)-V\left(\mathbf{r}-\frac{\mathbf{r}'}{2}\right)\right], \tag{2}$$

and the effect of electron or phonon coupling is described by the collision term

$$Cf_w(\mathbf{r},\mathbf{k},n,n',t)=F(\mathbf{q})\left\{e^{i\mathbf{q}\mathbf{r}}\left[\sqrt{n+1}f_w\left(\mathbf{r},\mathbf{k}-\frac{\mathbf{q}}{2},n+1,n',t\right)-\sqrt{n'}f_w\left(\mathbf{r},\mathbf{k}+\frac{\mathbf{q}}{2},n,n'-1,t\right)\right]+e^{-i\mathbf{q}\mathbf{r}}\left[-\sqrt{n}f_w\left(\mathbf{r},\mathbf{k}+\frac{\mathbf{q}}{2},n-1,n',t\right)+\sqrt{n'+1}f_w\left(\mathbf{r},\mathbf{k}-\frac{\mathbf{q}}{2},n,n'+1,t\right)\right]\right\} \tag{3}$$

(with the notations of Ref. 23).

If the coupling to the phonon mode is assumed to be weak, scattering phenomena involving several phonons are negligible and only consecutive phonon numbers are coupled through the generalized Wigner function. One can thus assume $f_w(\mathbf{r},\mathbf{k},n,n',t)=0$ if $|n-n'|>1$. If phonon-scattering phenomena are assumed to be more rapid than other phenomena at play (namely, the time-dependence of the Wigner function and the transport of carriers along the device), one can show, after a derivation inspired by that of Ref. 35 and detailed in the Appendix A,

$$\left(\frac{\partial}{\partial t}+\frac{\hbar\mathbf{k}}{m}\frac{\partial}{\partial\mathbf{r}}-Q\right)f_w(\mathbf{r},\mathbf{k},n,n,t)=2\pi\hbar F^2(\mathbf{q})\{\delta[E_0-E(\mathbf{k})+E(\mathbf{k}-\mathbf{q})](n+1)\times[f_w(\mathbf{r},\mathbf{k}-\mathbf{q},n+1,n+1,t)-f_w(\mathbf{r},\mathbf{k},n,n,t)]+\delta[E_0+E(\mathbf{k})-E(\mathbf{k}+\mathbf{q})]n\times[f_w(\mathbf{r},\mathbf{k}+\mathbf{q},n-1,n-1,t)-f_w(\mathbf{r},\mathbf{k},n,n,t)]\}. \tag{4}$$

This is a strong approximation that neglects advanced effects of electron or phonon coupling as collisional broadening and retardation or intracollisional field effects. It becomes wrong for devices operating at very high frequency.[35]

If we now consider the phonon mode to be itself coupled to an efficient thermostat so that the phonon mode remains in equilibrium every time we may consider that the generalized Wigner function factorizes as in Refs. 23 and 35

$$f_w(\mathbf{r},\mathbf{k},n,n,t) = f_w(\mathbf{r},\mathbf{k},t)\frac{1}{\bar{n}+1}\exp\left(-n\frac{\hbar\omega_0}{kT}\right), \tag{5}$$

where we have introduced the average phonon number $\bar{n} = [\exp(\hbar\omega_0/kT)-1]^{-1}$ and the reduced Wigner function of the electron system $f_w(\mathbf{r},\mathbf{k},t)$.

The transport equation of the reduced Wigner function is then obtained by tracing Eq. (4) over the phonon numbers

$$\begin{aligned}\left(\frac{\partial}{\partial t}+\frac{\hbar\mathbf{k}}{m}\frac{\partial}{\partial\mathbf{r}}-Q\right)f_w(\mathbf{r},\mathbf{k},t) &= 2\pi\hbar F^2(\mathbf{q})\{\delta[E_0-E(\mathbf{k})+E(\mathbf{k}-\mathbf{q})] \\ &\times[\bar{n}f_w(\mathbf{r},\mathbf{k}-\mathbf{q},t)-(\bar{n}+1)f_w(\mathbf{r},\mathbf{k},t)] \\ &+\delta[E_0+E(\mathbf{k})-E(\mathbf{k}+\mathbf{q})][(\bar{n}+1)f_w(\mathbf{r},\mathbf{k}+\mathbf{q},t) \\ &-\bar{n}f_w(\mathbf{r},\mathbf{k},t)]\}.\end{aligned} \tag{6}$$

In the presence of many phonon modes $\mathbf{q}$, it is straightforward to show that Eq. (6) may be generalized, leading to the equation known as the Wigner-Boltzmann equation[29]

$$\begin{aligned}\left(\frac{\partial}{\partial t}+\frac{\hbar\mathbf{k}}{m}\frac{\partial}{\partial\mathbf{r}}-Q\right)f_w(\mathbf{r},\mathbf{k},t) &= \sum_{\mathbf{q}} 2\pi\hbar F^2(\mathbf{q})\{\delta[E_0-E(\mathbf{k})+E(\mathbf{k}-\mathbf{q})] \\ &\times[\bar{n}f_w(\mathbf{r},\mathbf{k}-\mathbf{q},t)-(\bar{n}+1)f_w(\mathbf{r},\mathbf{k},t)] \\ &+\delta[E_0+E(\mathbf{k})-E(\mathbf{k}+\mathbf{q})] \\ &\times[(\bar{n}+1)f_w(\mathbf{r},\mathbf{k}+\mathbf{q},t)-\bar{n}f_w(\mathbf{r},\mathbf{k},t)]\}.\end{aligned} \tag{7}$$

In this approach the quantum dynamics of the electrons is thus accurately modeled. The main approximation is in the treatment of scattering phenomena. They are assumed to be fast and are finally modeled in the transport equation using the same term as in semiclassical transport.

B. Comparison with the quantum Brownian motion

We can now remark that this derivation strictly follows the general approach to quantum decoherence: it considers a supersystem including the system of interest (the electron) and its environment (the phonon mode in this case) with which the electron interacts. The master equation of the density matrix or the Wigner function of the system of interest is obtained by tracing the density matrix over the environment. To highlight the connection with the theory of quantum decoherence and to anticipate further remarks, it is insightful to look for a connection with the quantum Brownian motion, which is a simple and widely studied decoherence situation.[36] To this aim, we consider a simplified case where a one-dimensional (1D) electron interacts with numerous 1D phonon modes (as in a nanowire or a carbon nanotube) whose wave vectors q are much smaller than the typical values of electron wave vector k. The energy of the phonon modes is also assumed much smaller than the thermal energy kT so that $\bar{n}+1\approx\bar{n}$. In this case Eq. (6) simplifies to

$$\begin{aligned}\left(\frac{\partial}{\partial t}+\frac{\hbar k}{m}\frac{\partial}{\partial x}-Q\right)f_w(x,k,t) &= \sum_q 2\pi\hbar F^2(\mathbf{q})\bar{n}(q)\left[\delta\left(\hbar\omega_0(q)-\hbar^2\frac{kq}{m}\right)\right. \\ &\left.\times\{[f_w(x,k-q,t)+f_w(x,k+q,t)]-2f_w(x,k,t)\}\right],\end{aligned} \tag{8}$$

which may be approximated as

$$\left(\frac{\partial}{\partial t}+\frac{\hbar k}{m}\frac{\partial}{\partial x}-Q\right)f_w(x,k,t) = \left[\sum_q 2\pi\hbar F^2(\mathbf{q})q^2\bar{n}(q)\delta\left(\hbar\omega_0(q)-\hbar^2\frac{kq}{m}\right)\right]\frac{\partial^2 f_w(x,k,t)}{\partial k^2}. \tag{9}$$

The last term is reminiscent of the Fokker-Planck equation and is a form of the well-known equation of quantum Brownian motion.[36] In the most simple case, where the quantity $\Lambda=\Sigma_q 2\pi\hbar F^2(\mathbf{q})q^2\bar{n}(q)\delta[\hbar\omega_0(q)-\hbar^2\frac{kq}{m}]$ may be considered as k independent, it is well known that the Fokker-Planck equation leads to the exponential suppression of the nondiagonal terms of the electron-density matrix as $\rho(r,r';t)=\rho(r,r';0)e^{-\Lambda(r-r')^2t}$ and thus leads to an efficient spatial localization of the electrons.[36] This illustrates how phonon scattering may lead to localization, similarly to the case of particles subject to quantum Brownian motion. However, if Eq. (9) is insightful to understand how phonons can induce decoherence in electron devices it is probably insufficient to model decoherence accurately, as shown later on, since in semiconductor devices operating at room temperature the phonon wave vectors cannot be considered smaller than that of electrons and the phonon energies are comparable to the thermal energy kT. In contrast, directly solving the Wigner-Boltzmann Eq. (6) should provide a detailed description of phonon-induced decoherence in devices. In Sec. III we will compare the coherence length determined by these two approaches in gallium arsenide (GaAs) at room temperature.

C. Solution of the Wigner-Boltzmann equation

Different techniques to solving the Wigner-Boltzmann Eq. (6) have been developed. The direct solution may be obtained,[28,33,37–41] but its practical implementation is limited by some issues regarding the discretization of the derivative term[42] due to the highly oscillatory nature of the WF. The strong similarity with Boltzmann's equation suggests using statistical particle techniques in solving the Wigner transport equation as successfully and widely developed in the semiclassical case. The Monte Carlo treatment of both Q and C terms has been theorized and reported.[29] The corresponding algorithm suffers from the problem of exponential growth of the integer weight of particles, which can be successfully overcome by using a multiplication and recombination technique.[29,43] Another Wigner Monte Carlo technique con-

sists in treating statistically only the collision term. The quantum evolution term is considered through its effect on a new real parameter associated with each particle, the affinity, which contains the full wave properties of the electron system. Initially proposed by Shifren *et al.*,[27] it has been improved by the authors for the fully self-consistent simulation of resonant tunneling diodes and nanoscaled metal-oxide-semiconductor field effect transistors.[30–32] It is here employed to study electron decoherence in some structures and devices.

III. APPLICATION OF THE WIGNER-BOLTZMANN EQUATION TO THE EVOLUTION OF A FREE WAVE PACKET

To understand the mechanisms of decoherence we first simulate the evolution of an initially pure Gaussian state $\psi(x)=Ne^{-[(x-x_0)^2/2\sigma^2]}e^{ik_0x}$, which corresponds to an initial Wigner function $f_w(x,k)=N'e^{-[(x-x_0)^2/\sigma^2]}e^{-(k-k_0)^2\sigma^2}$, through the Wigner transport equation (N and N' are normalization constants). The initial transverse momentum of particles is randomly selected according to a thermal law. The semiconductor material is bulk three-dimensional gallium arsenide (GaAs) and the temperature is 300 K. The band-structure description is limited to the Γ valley and the scattering mechanisms considered are interactions with elastic acoustic phonons and inelastic polar optical phonons through standard parameters.[44]

The time-dependent electron Wigner function can be obtained directly from the Monte Carlo simulation.[30,31] The reduced density matrix $\rho(x,x')$ of electrons can be computed from the Wigner functions by inverse differential Fourier transform of the Wigner function as

$$\rho(x,x') = \int dk e^{ik(x-x')} f_w\left(\frac{x+x'}{2},k\right). \tag{10}$$

Computing the density matrix is insightful since its nondiagonal elements make obvious which positions of the real space are coherently connected.

Figures 1(a) and 1(b) show the cartography of the Wigner function and the modulus of the density matrix (DM), respectively, associated with the initial state defined by $k_0=4\times10^8$ m^{-1}, $\sigma=10$ nm. Figures 1(c) and 1(e) display the Wigner function of the wave packet after 130 fs of ballistic (no phonon) and diffusive (with phonons) propagation, respectively. Phonon scattering tends to widespread the WF over smaller k and displacement values [Fig. 1(e)] than in the purely coherent case [Fig. 1(c)]. The density matrix is plotted in the same situations in Figs. 1(d) and 1(f). In the ballistic case [Fig. 1(d)] all diagonal and nondiagonal elements grow from the initial state according to the natural coherent extension of the wave packet. When including scattering [Fig. 1(f)], the diagonal terms still grow similarly but they extend over a larger range, as indicated by the distribution tail at small x values. However, the nondiagonal elements do not extend as in the coherent case. They actually reduce as function of time.

To better quantify this behavior and the decoherence effect, we now consider two parameters: the purity of the density matrix and the coherence length of the wave packet.

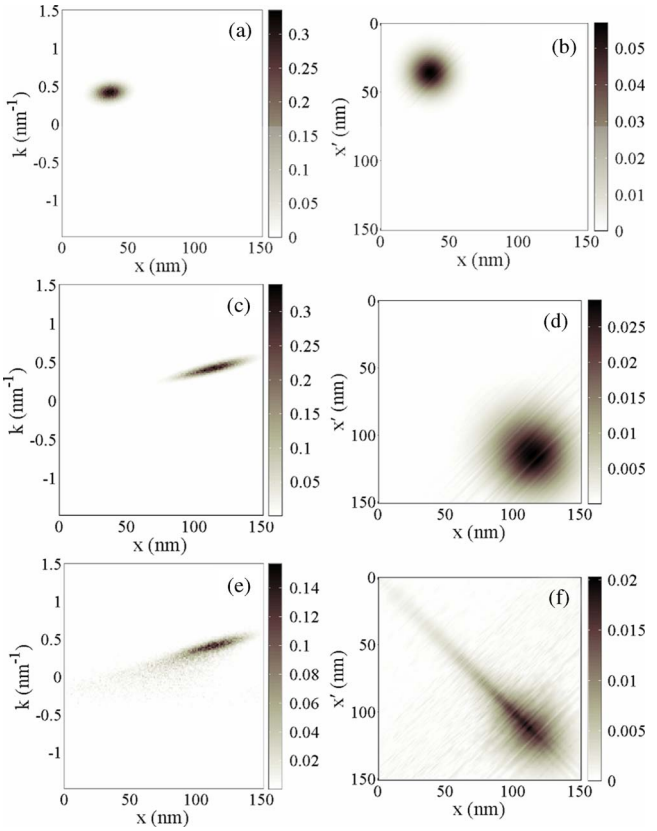

FIG. 1. (Color online) Evolution of a free wave packet coupled or uncoupled with a phonon bath at room temperature in GaAs. (a) Wigner function and (b) modulus of the density matrix of the initial pure state. Simulated WF and DM after 130 fs without (c) and (d) or with (e) and (f) coupling to the phonon bath. DM elements are expressed in nm^{-1}.

The purity of the density matrix $P=\mathrm{Tr}\,\rho^2$ which is equivalent to $P=2\pi\int dx\int dk f_w^2(x,k)$ (as defined in Ref. 45) is plotted in the inset of Fig. 2 as a function of time for different values of σ. A rapid decrease from the initial value of 1 (which characterizes a pure state) is observed at short times, almost independently of σ; the originally pure state rapidly evolves to a mixed state. At longer times the purity slowly converges to zero.

We plot in Fig. 2 (straight lines) the coherence length associated with the density matrix, which represents the typical length on which the construction of interferences is possible. It is estimated according to the traditional definition in quantum decoherence theory by $\rho(x+\frac{L_{\mathrm{coh}}}{2}x-\frac{L_{\mathrm{coh}}}{2})=e^{-1/8}\rho(x,x)$, as in Ref. 36.

The coherence length evolution is shown for wave packets with initial expansion σ of 5, 10, and 30 nm and initial zero average wave vector k_0. The theoretical coherence length at thermal equilibrium $L_{\mathrm{eq}}=\hbar/\sqrt{4mkT}$ is also shown on a horizontal dashed line for comparison.

Initially, the coherence length is equal to $\sigma/\sqrt{2}$. For a purely coherent situation, the coherence length should increase linearly with time. By contrast, in the presence of phonon coupling, it is observed that after about 100 fs, the coherence lengths for the three values of σ converge to a

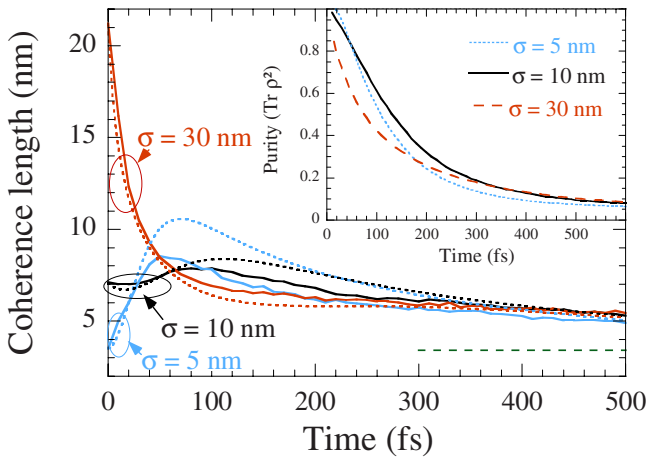

FIG. 2. (Color online) Coherence length of free wave packets that propagate with coupling to a phonon bath extracted from WMC simulation (straight lines) and corresponding quantum Brownian motion model (dotted lines) for different σ values. Horizontal line: theoretical thermal equilibrium coherence length. Inset: purity extracted from WMC simulation.

similar law, in which the coherence length decreases slowly. At short time, the cases with σ of 5 and 10 nm exhibit a maximum in the coherence length: the coherent wave-packet expansion is briefly stronger than decoherence.

These results are very reminiscent of the evolution of the free wave packet in quantum Brownian motion (QBM) theory, as reported for instance in Ref. 36. To highlight the comparison, the damping parameter Λ of a QBM model equivalent to Eq. (9) is fitted to give a long-time behavior similar to that resulting from Wigner Monte Carlo simulation. A value of $\Lambda=3.2\times10^{28}$ m^{-2} s^{-1} is found. It is remarkable that this value is consistent with the GaAs energy relaxation time γ^{-1}. QBM theory indeed predicts $\gamma=\Lambda\hbar^2/(mkT)$,[36] which gives $\gamma^{-1}=0.75$ ps, to be compared with $\gamma^{-1}\sim0.8$ ps in Ref. 46.

The coherence length evolution in QBM is superimposed to the Wigner Monte Carlo (WMC) extracted curves (dotted lines of Fig. 2). QBM model and WMC simulation indeed lead to similar behavior, but for small values of σ it is observed that the peak of coherence length is less pronounced with WMC simulation than with QBM model. This suggests that decoherence is faster for electrons in GaAs than for electrons subject to the QBM. This can be attributed to the existence of high-momentum (short-wavelength) phonons that localize electrons very efficiently in GaAs, whereas in QBM electrons are assumed to be scattered only by small momentum particles or fields.[36] Overall, this demonstrates that for a free propagation, scattering-induced decoherence rapidly dominates over the coherent expansion of the wave packet.

IV. INTERACTION OF A WAVE PACKET WITH SINGLE AND DOUBLE BARRIERS

We now consider a tunnel barrier because such a situation is able to build spatial quantum coherence: if a wave-packet is sent ballistically onto the barrier, the resulting reflected

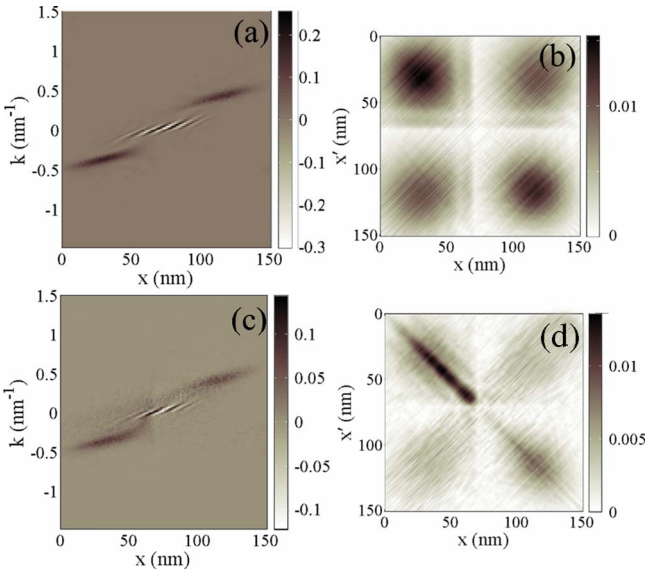

FIG. 3. (Color online) WF and modulus of the DM of a wave packet after interaction with a single barrier without (a) and (b) and with (c) and (d) coupling to a phonon bath. DM elements are expressed in nm^{-1}, the barrier is located at the position $x_c=75$ nm, and its width is 2 nm.

and transmitted wave packets are fully coherent with each other. This is well observed in Figs. 3(a) and 3(b) which show WF and DM in a situation where a Gaussian wave packet with $k_0=4\times10^8$ m^{-1}, $\sigma=10$ nm, and an initial central position $x_0=30$ nm has interacted with a tunnel barrier (the WF and DM are plotted after 130 fs). The barrier is located at the position $x_c=75$ nm (that is the center of the x axis), its width is 2 nm, and its energy height 0.3 eV.

Electrons on left and right sides of the barrier are fully coherent, so high nondiagonal values appear in the density matrix. This coherence manifests on the WF by strong positive and negative oscillations around $k=0$. In the presence of phonons [Figs. 3(c) and 3(d)], the coherence between left and right sides of the barrier appears strongly damped. The electrons are separately localized and if interferences between electrons on the left and right sides could be constructed, they would have low contrast.

To quantify the localization of electrons on one or the other side of the barrier due to decoherence it is insightful to introduce an evaluation of the coherence between the left (L) and the right (R) sides of the barrier by

$$C=\frac{\int_L dx\int_R dx'|\rho(x,x')|}{\int_L dx\rho^{1/2}(x,x)\int_R dx\rho^{1/2}(x,x)}. \quad (11)$$

This parameter compares the nondiagonal elements connecting the left and right sides of the barrier with the diagonal elements of the left and right sides and is equal to one for a purely coherent situation. It is plotted as a function of time in Fig. 4 for two k_0 values. It appears that coherence decreases rapidly: an electron that tunnels through a barrier can rapidly

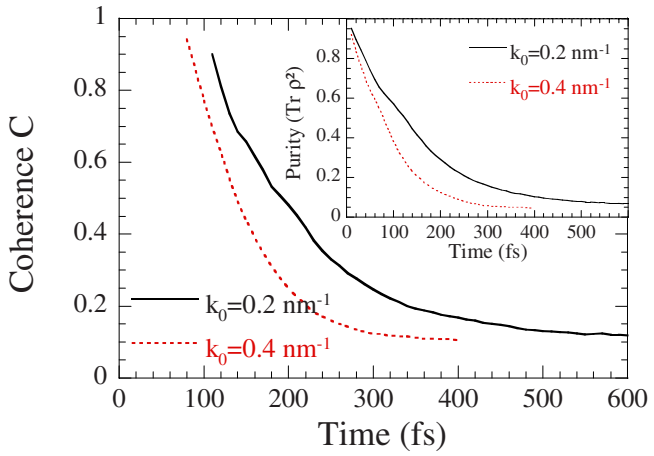

FIG. 4. (Color online) Coherence C [defined in Eq. (11)] between the two sides of the single barrier as a function of time after interaction of a wave packet with a single barrier, for two initial average wave vectors k_0. Inset: purity as a function of time in the same situations.

be considered as being on one side of the barrier, but not in a coherent state between the two states. In other words, the coherence between transmitted and reflected electrons is rapidly lost. The inset of Fig. 4 also shows the purity as a function of time: this parameter decreases rapidly with a rate depending on k_0.

We now examine the double-barrier case from the decoherence viewpoint. Double barriers are essential structures in nanoelectronics because they are present in many nanodevices (e.g., resonant tunneling diodes and transport through quantum dots or molecules) and have a strong conceptual significance. We consider a double barrier located centered around the position $x_c=75$ nm. Both barriers have a 1.5 nm width and a 0.3 eV energy height, and they are 5 nm apart. The same wave packet as for the single-barrier case is sent onto the double barrier and the DM is plotted after 130 fs. Figure 5(a) shows the DM in a situation with no decoherence. A part of the wave packet is trapped in the quasibound state of the double barrier, while another part is reflected. The trapped part slowly leaks to the right side of the barrier. Vertical and horizontal lines at the position $x_c=75$ nm show the coherence between electrons trapped in the double barrier and electrons on the left or right side of the double barrier. The high nondiagonal values show the coherence of electrons between left and right sides of the double barrier. The transport is thus fully coherent: tunneling only occurs through the quasibound state in a resonant process. It is also interesting to notice a minimum of the density matrix for x around 50 nm, which is due to quantum inference.[47]

When including phonon scattering [Fig. 5(b)] the process appears significantly different and the coherence is strongly reduced between electrons in the quasibound states and electrons on left or right side of the barrier. This is well illustrated on Fig. 5(c) where a cut of the density-matrix elements along the central position of the double barrier $x_c=75$ nm is plotted, with and without coupling to the phonons bath. The population at x_c $\rho(x_c,x_c)$ is almost independent of the presence of the phonon bath, whereas the coherences with the

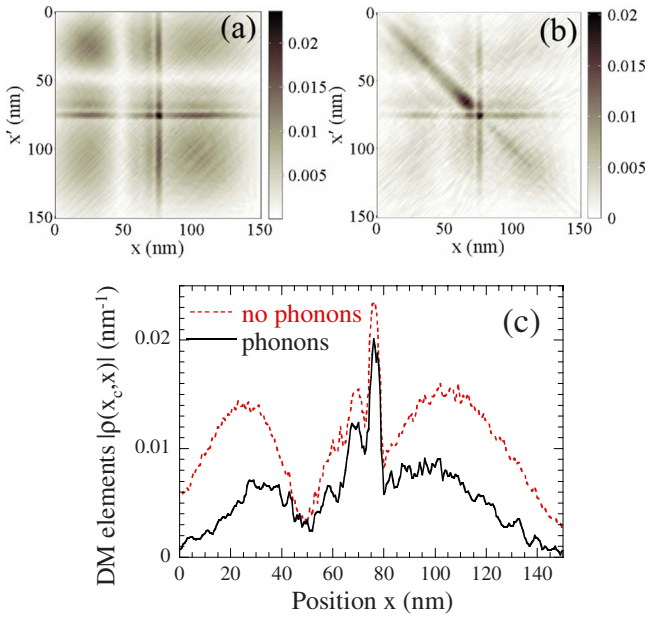

FIG. 5. (Color online) Modulus of the DM of a wave packet after interaction with a double barrier without (a) and with (b) coupling to a phonon bath (expressed in nm^{-1}). The double barrier is centered around $x_c=75$ nm, barriers have a 1.5 nm width, and are 5 nm apart. (c) Modulus of the DM elements at the central position of the double barrier $|\rho(x_c,x)|$ ($x_c=75$ nm) for both situations.

left and right sides of the double barrier $\rho(x_c,x)$ are strongly damped by the presence of the phonon bath. It appears that many electrons trapped in the quasibound state interact with phonons before leaving this state and are thus localized before exiting. Additionally, the coherence between electrons on left and right sides has almost disappeared. The process of double-barrier tunneling is thus no longer fully resonant. Electrons can be seen as entering and leaving the quasibound state in distinct processes, with the possibility of energy exchange with the phonons. This illustrates the well-known coherent vs sequential tunneling situation, which is very important for resonant tunneling diode operation.[14,48]

V. PHONON-INDUCED DECOHERENCE IN RESONANT TUNNELING DIODE

We now turn to the simulation of an actual device connected to external circuit by ohmic contacts: the resonant tunneling diode (RTD). The Wigner Monte Carlo algorithm coupled to Poisson's equation is very well adapted to the simulation of resonant tunneling diodes. In the ballistic case it gives the same result as the NEGF technique and when including phonon scattering it gives results consistent with experiments at 300 and 77 K, as demonstrated in Ref. 30. The detailed boundary and injection conditions implemented in the device simulator are described and validated in Refs. 30 and 31. The active structure consists of a 5 nm thick GaAs quantum well embedded in 3 nm thick AlGaAs barriers and 9.5 nm thick GaAs buffer layers. On both sides 50 nm long access regions are doped to 10^{18} cm^{-3}. In addition to polar optical and acoustic phonon scattering in the whole

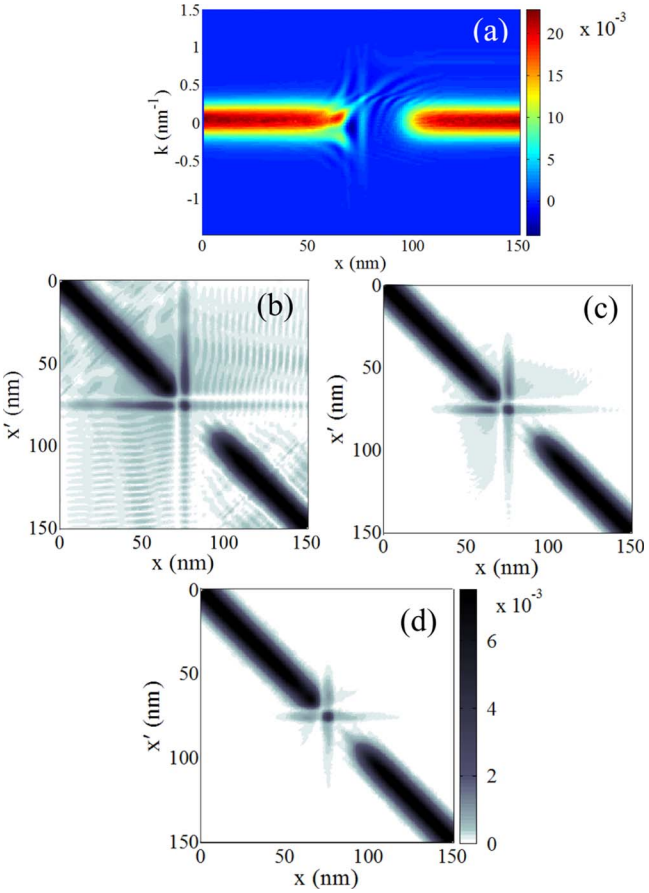

FIG. 6. (Color online) (a) WF of a RTD operating at peak voltage. (b)–(d) Modulus of the DM of a RTD operating at peak voltage (no scattering, standard phonon-scattering rates, standard rates multiplied by 5) expressed in nm^{-1}.

structure, ionized impurity scattering in these access regions is also included in the Monte Carlo transport algorithm.[30]

Figure 6(a) shows the WF of the RTD operating at peak voltage (V=0.3 V). The transport in a large part of access regions ($x<30$ nm and $x>120$ nm) is essentially semiclassical and the WF matches very well a distribution function represented by a displaced Maxwellian function (not shown explicitly). Inside the quantum well the WF around k=0 is similar to that of the WF of the first bound state in a square potential.[30] In the overall active region of the device, oscillations of the WF reveal the presence of spatial coherence. This coherence and the phonon-induced decoherence are highlighted in Figs. 6(b)–6(d) which represent the density matrix in three different scattering situations. In Fig. 6(b) the transport is fully ballistic in the active region, which means that phonon scattering has been artificially switched off. In Fig. 6(c) standard scattering rates were used as for the WF plotted in Fig. 6(a). In Fig. 6(d) phonon-scattering rates have been multiplied by 5.

In the ballistic case [Fig. 6(b)], a strong coherence is observed between electrons in the quantum well and in the emitter region. Nondiagonal elements are also significant between electrons in collector and emitter regions, which is an indication of a coherent transport regime. When including standard scattering rates, the nondiagonal elements strongly

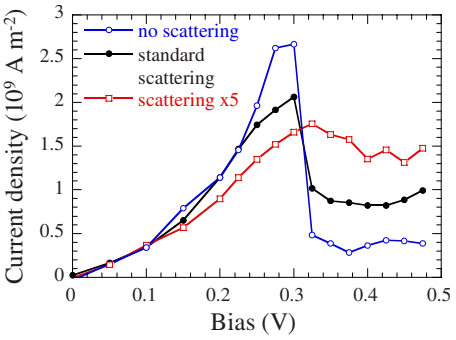

FIG. 7. (Color online) Simulated current versus voltage of a RTD with no scattering, standard scattering, and scattering rates multiplied by 5 in the active region.

reduce and the coherences almost fully disappear when phonon-scattering rates are multiplied by 5. In this case nondiagonal elements of the DM almost entirely vanish, which indicates that the system is now in the sequential tunneling regime. This phonon-induced transition between coherent and sequential tunneling regimes manifests itself in the current-voltage characteristics of the RTD plotted in Fig. 7 for the three scattering situations. Phonon scattering tends to suppress the resonant tunneling peak while the valley current increases to such a point that the negative differential conductance effect almost disappears. The device tends to behave as a simple tunneling resistance for which a semiclassical-type description could be accurate enough.

All these considerations give a clear view of how electrons are delocalized in the active part of the device and become more localized again in the access region. This seems to suggest a transition from "quantum" to "semiclassical" transport from the active region to the access, which has been suggested and discussed in different works[11,28] and is here observed directly. To illustrate this statement, it is insightful to couple a semiclassical Boltzmann transport equation solution in the access regions with a Wigner transport equation solution in the quantum region. This is easily achieved using our algorithm.[30,31,49] In Fig. 8, the I-V curve of the resonant tunneling diode simulated only using Wigner Monte Carlo simulation is plotted, together with I-V curves obtained using coupled Boltzmann and Wigner simulations, with different locations of the Boltzmann or Wigner boundary. When the boundary is set to 50 nm from the tunnel barriers, the I-V curve is superimposed with the full Wigner simulation, suggesting that at 50 nm from the double barrier, electrons have acquired a fully semiclassical behavior. However when the boundary is set to 10 nm, and even more to 5 nm, the I-V curve is strongly affected. This is consistent with the density matrix of Fig. 6(c) that shows that the delocalization of the electrons extends beyond 10 nm from the double barrier. Treating the electrons as semiclassical in this region thus logically leads to unphysical results. This set of results shows it is possible to separate "quantum" and "semiclassical" regions in nanoscaled electron devices. It also highlights that when simulating long access regions including the effects of scattering, the particles are in semiclassical states at the contacts.

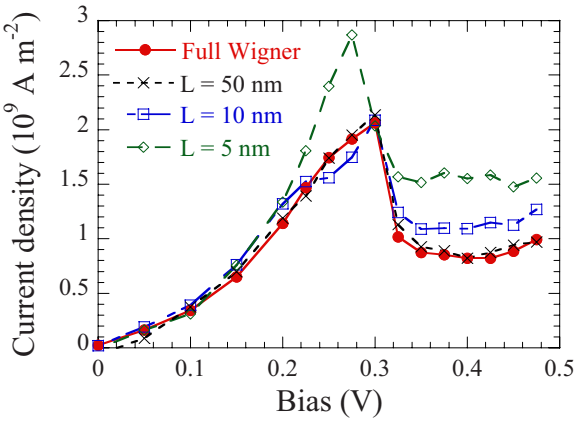

FIG. 8. (Color online) Coupled Wigner and Boltzmann simulation of current versus voltage of a RTD for different positions of the semiclassical or quantum boundary L (the quantum region extends to a distance L before and after the barriers).

VI. CONCLUSION

In this paper, the phenomena related to phonon-induced decoherence in semiconductor nanostructures and devices were investigated using state-of-the-art quantum simulation based on a Wigner Monte Carlo algorithm. The Wigner-Boltzmann transport equation was first established as an appropriate framework for such a study, especially thanks to its close connection with the semiclassical Boltzmann approach and to its straightforward relationship with the density matrix whose diagonal elements provide a clear view of the coherence evolution in the device. By analyzing the behavior of a free wave packet in GaAs at room temperature it was then emphasized that decoherence rapidly dominates and suppresses the coherent expansion of the wave packet, even faster than in the commonly studied model of quantum Brownian motion. In the case of an electron wave packet interacting with a tunneling barrier it was shown that phonon scattering strongly localizes electrons on one or the other side the barrier, which makes the coherence between reflected and transmitted waves vanishing. In a double-barrier structure, compared to ballistic transport, it was clearly shown how the phonon-induced decoherence may cause the transition, at least partially, from coherent to sequential tunneling. The decoherence effect was then studied in the realistic case of the resonant tunneling diode. Starting from the ballistic limit it was shown that when increasing the phonon-scattering rates the negative differential conductance behavior is progressively lost, which makes the resonant-device behavior like that of a simple tunneling resistance. Finally, taking advantage of the full compatibility between Boltzmann and Wigner Monte Carlo transport algorithms, the transition between semiclassical and quantum regions of the RTD was investigated. In particular, according to the coherence length, it was shown that for long enough access regions the particles can be actually considered as semiclassical near contacts. This set of results helps understanding how phonon-induced decoherence and electron localization occur in semiconductor nanodevices operating at room temperature and whether quantum phenomena can take place or not. The Wigner formalism used throughout this works appears to be useful and relevant for the quantitative analysis of electron decoherence and for the investigation of solid-state devices operating in mixed quantum/semiclassical regime.

ACKNOWLEDGMENTS

The authors would like to thank V.-N. Do, K. Huet, and A. Valentin for fruitful discussions and the anonymous reviewers for their very helpful comments. This work was partly supported by EC through the NANOSIL Network of Excellence and the PULLNANO Integrated Project (Contract No. IST 4-026828), and by the French ANR through project MODERN.

APPENDIX

For the phonon coordinates diagonal terms of the generalized Wigner function, Eq. (3) gives (cc is the complex conjugate of the right-hand side)

$$\left(\frac{\partial}{\partial t}+\frac{\hbar\mathbf{k}}{m}\frac{\partial}{\partial\mathbf{r}}-Q\right)f_w(\mathbf{r},\mathbf{k},n,n,t)$$
$$=F(\mathbf{q})\left\{e^{i\mathbf{qr}}\left[\sqrt{n+1}f_w\left(\mathbf{r},\mathbf{k}-\frac{\mathbf{q}}{2},n+1,n,t\right)\right.\right.$$
$$\left.\left.-\sqrt{n}f_w\left(\mathbf{r},\mathbf{k}+\frac{\mathbf{q}}{2},n,n-1,t\right)\right]\right\}+\text{cc}. \tag{A1}$$

The evolution of the phonon coordinates off-diagonal component $f_w[\mathbf{r},\mathbf{k}-(\mathbf{q}/2),n+1,n,t]$ [appearing in Eq. (A1)] is given by, under the weak-coupling approximation,

$$\left(\frac{\partial}{\partial t}+\frac{\hbar\mathbf{k}}{m}\frac{\partial}{\partial\mathbf{r}}+i\omega_0-Q\right)f_w(\mathbf{r},\mathbf{k},n+1,n,t)$$
$$=F(\mathbf{q})\left\{e^{-i\mathbf{qr}}\left[-\sqrt{n+1}f_w\left(\mathbf{r},\mathbf{k}+\frac{\mathbf{q}}{2},n,n,t\right)\right.\right.$$
$$\left.\left.+\sqrt{n+1}f_w\left(\mathbf{r},\mathbf{k}-\frac{\mathbf{q}}{2},n+1,n+1,t\right)\right]\right\}. \tag{A2}$$

We perform the classical variable substitution[50]

$$\left\{\begin{array}{l}\mathbf{r}(t)=\mathbf{r}'(t')+\dfrac{\hbar\mathbf{k}}{m}(t-t')\\ t'=t\end{array}\right., \tag{A3}$$

so that Eq. (A2) becomes

$$\left(\frac{\partial}{\partial t'}+i\omega_0-Q\right)f_w(\mathbf{r}',\mathbf{k},n+1,n,t)$$
$$=F(\mathbf{q})\left\{e^{-i\mathbf{qr}}\left[-\sqrt{n+1}f_w\left(\mathbf{r}'(t),\mathbf{k}+\frac{\mathbf{q}}{2},n,n,t\right)\right.\right.$$
$$\left.\left.+\sqrt{n+1}f_w\left(\mathbf{r}'(t),\mathbf{k}-\frac{\mathbf{q}}{2},n+1,n+1,t\right)\right]\right\}. \tag{A4}$$

Equation (A4) is then directly integrated

$$f_w(\mathbf{r},\mathbf{k},n+1,n,t) = ic + e^{-i\omega_0 t}\int_0^t dt' F(\mathbf{q}) e^{i\mathbf{q}\mathbf{r}'(t')+i\omega_0 t'} \times\left[-\sqrt{n+1} f_w\left(\mathbf{r}'(t'),\mathbf{k}+\frac{\mathbf{q}}{2},n,t'\right) + \sqrt{n+1} f_w\left(\mathbf{r}'(t'),\mathbf{k}-\frac{\mathbf{q}}{2},n+1,t'\right)\right] + e^{-i\omega_0 t}\int_0^t dt' e^{i\omega_0 t'} Q f_w[\mathbf{r}'(t'),\mathbf{k},n+1,n,t']. \quad \text{(A5)}$$

The electron and phonon are assumed initially uncoupled so that the initial condition (ic) can be assumed to be zero. It is then straightforward to derive the counterpart of Eq. (A5) for $f_w(\mathbf{r},\mathbf{k},n,n-1,t)$. The integral expressions of $f_w(\mathbf{r},\mathbf{k},n+1,n,t)$ and $f_w(\mathbf{r},\mathbf{k},n,n-1,t)$ can be injected into Eq. (A1):

$$\left(\frac{\partial}{\partial t}+\frac{\hbar\mathbf{k}}{m}\frac{\partial}{\partial\mathbf{r}}-Q\right)f_w(\mathbf{r},\mathbf{k},n,t) = F^2(\mathbf{q})\int_0^t dt' e^{i\mathbf{q}\mathbf{r}}(n+1)e^{-i\omega_0 t - i\mathbf{q}\mathbf{r}'(t')+i\omega_0 t'} \times\{-f_w[\mathbf{r}'(t'),\mathbf{k},n,t'] + f_w[\mathbf{r}'(t'),\mathbf{k}-\mathbf{q},n+1,t']\} + dt' e^{i\mathbf{q}\mathbf{r}} n e^{-i\omega_0 t - i\mathbf{q}\mathbf{r}''(t')+i\omega_0 t'}\{f_w[\mathbf{r}''(t'),\mathbf{k}+\mathbf{q},n-1,t'] - f_w[\mathbf{r}''(t'),\mathbf{k},n,t']\} + \mathrm{ICF} + \mathrm{cc}, \quad \text{(A6)}$$

where $\mathbf{r}(t)=\mathbf{r}'(t')+\hbar(\mathbf{k}-\mathbf{q}/2)(t-t')/m$ and $\mathbf{r}(t)=\mathbf{r}''(t')+\hbar(\mathbf{k}+\mathbf{q}/2)(t-t')/m$ and we have introduced the intracollisional field effect term

$$\mathrm{ICF} = F(\mathbf{q})e^{i\mathbf{q}\mathbf{r}} \times\left[\sqrt{n+1}e^{-i\omega_0 t}\int_0^t dt' e^{i\omega_0 t'} Q f_w\left(\mathbf{r}'(t'),\mathbf{k}-\frac{\mathbf{q}}{2},n+1,n,t'\right) - \sqrt{n}e^{-i\omega_0 t}\int_0^t dt' e^{i\omega_0 t'} Q f_w\left(\mathbf{r}''(t'),\mathbf{k}+\frac{\mathbf{q}}{2},n,n-1,t'\right)\right]. \quad \text{(A7)}$$

The exponentials in Eq. (A6) are then factorized and transformed by introducing the energies $E(\mathbf{k})$, $E(\mathbf{k}-\mathbf{q})$, and $E(\mathbf{k}+\mathbf{q})$:

$$\left(\frac{\partial}{\partial t}+\frac{\hbar\mathbf{k}}{m}\frac{\partial}{\partial\mathbf{r}}-Q\right)f_w(\mathbf{r},\mathbf{k},n,t) = F^2(\mathbf{q})\int_0^t dt'(n+1)e^{\frac{i}{\hbar}[E_0-E(\mathbf{k})+E(\mathbf{k}-\mathbf{q})](t-t')} \times\{-f_w[\mathbf{r}'(t'),\mathbf{k},n,t'] + f_w[\mathbf{r}\,'(t'),\mathbf{k}-\mathbf{q},n+1,t']\} + dt' n e^{\frac{i}{\hbar}[E_0+E(\mathbf{k})-E(\mathbf{k}+\mathbf{q})](t-t')}\{f_w[\mathbf{r}''(t'),\mathbf{k}+\mathbf{q},n-1,t'] - f_w[\mathbf{r}''(t'),\mathbf{k},n,t']\} + \mathrm{ICF} + \mathrm{cc}. \quad \text{(A8)}$$

This equation is still exact in the weak-coupling limit and includes all finite collision time effects (collision broadening and retardation, intracollision field effect). If the phonon scattering is assumed rapid regarding to the transport phenomena, as explained in the body text, we may use the relation demonstrated in Ref. 51 (p.v. refers to the Cauchy principal value)

$$\int_0^t dt' e^{i\omega(t'-t)}\Phi(t') \approx \Phi(t)\left(\pi\delta(\omega)+i\,\mathrm{p.v.}\,\frac{1}{\omega}\right). \quad \text{(A9)}$$

All the principal values cancel each other. The intracollisional field effect term gives a contribution that is proportional to $\delta(\omega_0)$, which vanishes since the phonon has a nonzero energy. This thus leads directly to Eq. (4).

*Corresponding author. FAX: +3 316 915 4020:
damien.querlioz@ief.u-psud.fr

[1] D. K. Ferry, R. Akis, and J. P. Bird, Phys. Rev. Lett. **93**, 026803 (2004).
[2] I. Knezevic, Phys. Rev. B **77**, 125301 (2008).
[3] F. Buscemi, P. Bordone, and A. Bertoni, Phys. Status Solidi C **5**, 139 (2008).
[4] H. M. Pastawski, L. E. F. Foa Torres, and E. Medina, Chem. Phys. **281**, 257 (2002).
[5] F. Buscemi, E. Cancellieri, P. Bordone, A. Bertoni, and C. Jacoboni, Phys. Status Solidi C **5**, 52 (2008).
[6] In this work, electron localization refers to the reduction of the extension of the wave packet caused by the environment and is very different from the weak or strong localization caused by disorder.
[7] R. Brunetti, C. Jacoboni, and F. Rossi, Phys. Rev. B **39**, 10781 (1989).
[8] C. Jacoboni, Semicond. Sci. Technol. **7**, B6 (1992).
[9] F. Rossi and C. Jacoboni, EPL **18**, 169 (1992).
[10] M. V. Fischetti, J. Appl. Phys. **83**, 270 (1998).
[11] M. V. Fischetti, Phys. Rev. B **59**, 4901 (1999).
[12] R. Gebauer and R. Car, Phys. Rev. B **70**, 125324 (2004).
[13] W. R. Frensley, Rev. Mod. Phys. **62**, 745 (1990).
[14] M. Büttiker, IBM J. Res. Dev. **32**, 63 (1988).
[15] R. Venugopal, M. Paulsson, S. Goasguen, S. Datta, and M. S. Lundstrom, J. Appl. Phys. **93**, 5613 (2003).
[16] J. Wang, E. Polizzi, and M. Lundstrom, J. Appl. Phys. **96**, 2192 (2004).
[17] Z. Ren, R. Venugopal, S. Goasguen, S. Datta, and M. S. Lundstrom, IEEE Trans. Electron Devices **50**, 1914 (2003).
[18] J. L. D'Amato and H. M. Pastawski, Phys. Rev. B **41**, 7411 (1990).
[19] D. K. Ferry and S. M. Goodnick, *Transport in Nanostructures* (Cambridge University Press, Cambridge, England, 1997).
[20] S. Jin, Y. J. Park, and H. S. Min, J. Appl. Phys. **99**, 123719 (2006).

[21] A. Svizhenko and M. P. Anantram, IEEE Trans. Electron Devices **50**, 1459 (2003).
[22] E. Wigner, Phys. Rev. **40**, 749 (1932).
[23] A. Bertoni, P. Bordone, R. Brunetti, and C. Jacoboni, J. Phys.: Condens. Matter **11**, 5999 (1999).
[24] B. Vacchini and K. Hornberger, Eur. Phys. J. Spec. Top. **151**, 59 (2007).
[25] J. J. Halliwell, J. Phys. A: Math. Theor. **40**, 3067 (2007).
[26] N. Kluksdahl, W. Pötz, U. Ravaioli, and D. K. Ferry, Superlattices Microstruct. **3**, 41 (1987).
[27] L. Shifren, C. Ringhofer, and D. K. Ferry, IEEE Trans. Electron Devices **50**, 769 (2003).
[28] W. R. Frensley, Phys. Rev. B **36**, 1570 (1987).
[29] M. Nedjalkov, H. Kosina, S. Selberherr, C. Ringhofer, and D. K. Ferry, Phys. Rev. B **70**, 115319 (2004).
[30] D. Querlioz, P. Dollfus, V.-N. Do, A. Bournel, and V. Nguyen, J. Comput. Electron. **5**, 443 (2006).
[31] D. Querlioz, J. Saint-Martin, V. N. Do, A. Bournel, and P. Dollfus, IEEE Trans. Nanotechnol. **5**, 737 (2006).
[32] D. Querlioz, J. Saint-Martin, K. Huet, A. Bournel, V. Aubry-Fortuna, C. Chassat, S. Galdin-Retailleau, and P. Dollfus, IEEE Trans. Electron Devices **54**, 2232 (2007).
[33] B. A. Biegel and J. D. Plummer, Phys. Rev. B **54**, 8070 (1996).
[34] F. A. Buot and K. L. Jensen, Phys. Rev. B **42**, 9429 (1990).
[35] M. Nedjalkov, D. Vasileska, D. K. Ferry, C. Jacoboni, C. Ringhofer, I. Dimov, and V. Palankovski, Phys. Rev. B **74**, 035311 (2006).
[36] E. Joos, *Decoherence and the Appearance of a Classical World in Quantum Theory* (Springer-Verlag, Berlin, 2003), p. 41.
[37] K. L. Jensen and F. A. Buot, J. Appl. Phys. **67**, 2153 (1990).
[38] D. R. Miller and D. P. Neikirk, Tech. Dig. - Int. Electron Devices Meet. **1992**, 561.
[39] M. D. Croitoru, V. N. Gladilin, V. M. Fomin, J. T. Devreese, W. Magnus, W. Schoenmaker, and B. Soree, J. Appl. Phys. **93**, 1230 (2003).
[40] K.-Y. Kim, J. Appl. Phys. **102**, 113705 (2007).
[41] N. C. Kluksdahl, A. M. Kriman, D. K. Ferry, and C. Ringhofer, Phys. Rev. B **39**, 7720 (1989).
[42] K.-Y. Kim and B. Lee, Solid-State Electron. **43**, 2243 (1999).
[43] V. Sverdlov, T. Grasser, H. Kosina, and S. Selberherr, J. Comput. Electron. **5**, 447 (2006).
[44] K. Hess, *Monte Carlo Device Simulation: Full Band and Beyond* (Kluwer, Dordrecht, 1991).
[45] G. Manfredi and M. R. Feix, Phys. Rev. E **62**, 4665 (2000).
[46] M. V. Fischetti, IEEE Trans. Electron Devices **38**, 634 (1991).
[47] L. Shifren and D. K. Ferry, Phys. Lett. A **285**, 217 (2001).
[48] S. Datta, *Electronic Transport in Mesoscopic Systems* (Cambridge University Press, Cambridge, England, 1995).
[49] D. Querlioz, J. Saint-Martin, V.-N. Do, A. Bournel, and P. Dollfus, Tech. Dig. - Int. Electron Devices Meet. **2006**, 941.
[50] F. Rossi, P. Poli, and C. Jacoboni, Semicond. Sci. Technol. **7**, 1017 (1992).
[51] C. Ringhofer, H. Kosina, M. Nedjalkov, and S. Selberherr, SIAM J. Appl. Math. **64**, 1933 (2004).